Chapter 7

How Important is Metal-Carbon Back-Bonding for the Stability of Fullerene-Transition Metal Complexes? Role of Cage Sizes, Encapsulated Ions and Metal Ligands

Ming-Chung Yang and Ming-Der Su

Additional information is available at the end of the chapter

http://dx.doi.org/10.5772/intechopen.70068

Abstract

A density functional study of $\{\eta^2\text{-}(X@C_n)\}ML_2$ complexes with various cage sizes (C_{60}, C_{70}, C_{76}, C_{84}, C_{90}, C_{96}), encapsulated ions ($X = F^-$, 0, Li^+) and metal fragments (M = Pt, Pd) is performed, using M06/LANL2DZ levels of theory. The importance of π back-bonding to the thermodynamic stability of fullerene-transition metal complexes ($\{\eta^2\text{-}(X@C_n)\}ML_2$) and the effect of encapsulated ions, metal fragments and cage sizes on the π back-bonding are determined in this study. The theoretical computations suggest that π back-bonding plays an essential role in the formation of fullerene-transition metal complexes. The theoretical evidence also suggests that there is no linear correlation between cage sizes and π back-bonding, but the encapsulated Li^+ ion enhances π back-bonding and F^- ion results in its deterioration. These computations also show that a platinum center produces stronger π back-bonding than a palladium center. It is hoped that the conclusions that are provided by this study can be used in the design, synthesis and growth of novel fullerene-transition complexes.

Keywords: fullerene-transition metal complex, π back-bonding, encapsulated ions, metal fragments and cage sizes

1. Introduction

The first fullerene-transition metal complex, $(\eta^2\text{-}C_{60})Pt(Ph_3)_2$, was prepared and structurally characterized by Fagan et al. in 1991 [1]. It was the starting point for a new class of study for fullerene chemistry. Since then, various fullerene-transition metal complexes have been synthesized and these have potential applications in solar cells, spintronics, catalysis and

drug delivery [2]. Balch et al. then studied the reactions of C_{60} with electron-rich fragments, $IrCl(CO)(PPh_3)_2$ and produced the fullerene-iridium complex $(\eta^2\text{-}C_{60})IrCl(CO)(PPh_3)_2$ [3]. The formation of fullerene-iridium complex is a reversible process and the reversible binding of $IrCl(CO)(PPh_3)_2$ to fullerenes can be used as a structural probe because the adducts can build ordered single crystals that are suitable for X-ray diffraction [4, 5]. Fullerene-iridium complexes that contain an enantiomeric phosphine ligand are used as solar photoelements [6]. One of the significant characteristics of fullerenes is that they are capable of encaging atoms, ions and small molecules to form endohedral complexes. Endohedral metallofullerenes (EMFs) are those that encapsulate metal atoms within a hollow carbon cage. Proft et al. theoretically studied the interactions between encapsulated monoatomic ions (Li^+ to Rb^+ and F^- to I^-) and C_{60} and its Si and Ge analogues [7] and found that, for these families, the interactions between $Li^+(Na^+)$ and $F^-(Cl^-)$ ions and C_{60} are strongest and exothermic, which confirms the possibility of the existence of these species. Recently, $Li^+@C_{60}$ was successfully synthesized and isolated by Watanabe et al. [8].

Understanding the strength and nature of metal-ligand bonding is crucial for the design of new fullerene-transition metal complexes because the structure and stability of various intermediates are important to the formation of organometallics [9]. In an earlier work by the authors [10], $\{\eta^2\text{-}(X@C_{60})\}ML_2$ complexes (M = Pt, Pd; X = 0, Li^+, L = PPh_3) were studied and it was found that there is a relationship between thermodynamic stability and π back-bonding; that is, the greater the π back-bonding, the greater is thermodynamic stability. This shows that thermodynamic stability can be modified by tuning the π back-bonding. As far as the authors are aware, π back-bonding could be affected by several factors, including the encapsulated ions, the metal fragments and the cage sizes. This study determines the importance of π back-bonding to the thermodynamic stability of $\{\eta^2\text{-}(X@C_n)\}ML_2$ complexes by using M = Pt, Pd; X = F^-, 0, Li^+ and n = 60, 70, 76, 84, 90 and 96 to ascertain the role of these factors in π back-bonding. Since the system is very large, methyl-substituted N-heterocyclic carbenes (NHC) are used as a ligand (L), instead of PPh_3. NHC is one of the frequently used and most powerful tools in organic chemistry [11]. In this work, the following reactions are studied:

$$ML_2 + X@C_n \rightarrow \{\eta^2\text{-}(X@C_n)\}ML_2 \quad (1)$$

2. Computational details

The following fullerenes that comply with the isolated pentagon rule are used to develop a correlation: Ih-C_{60}, D_{5h}-C_{70}, D_2-C_{76}, $D_{2d}(23)$-C_{84}, $D_{5h}(1)$-C_{90} and $D_{3d}(3)$-C_{96}. These are experimentally isolated and identified [12–14]. The symmetry and numbering scheme for fullerene isomers are in accordance with an approved classification [15]. Hückel molecular orbital calculations show that the 6:6 ring junctions at the poles of the molecules usually have highest π bond orders (B) and are expected to be the most reactive, so these are the sites of attack (see **Scheme 1**) [12, 16].

http://dx.doi.org/10.5772/intechopen.70068

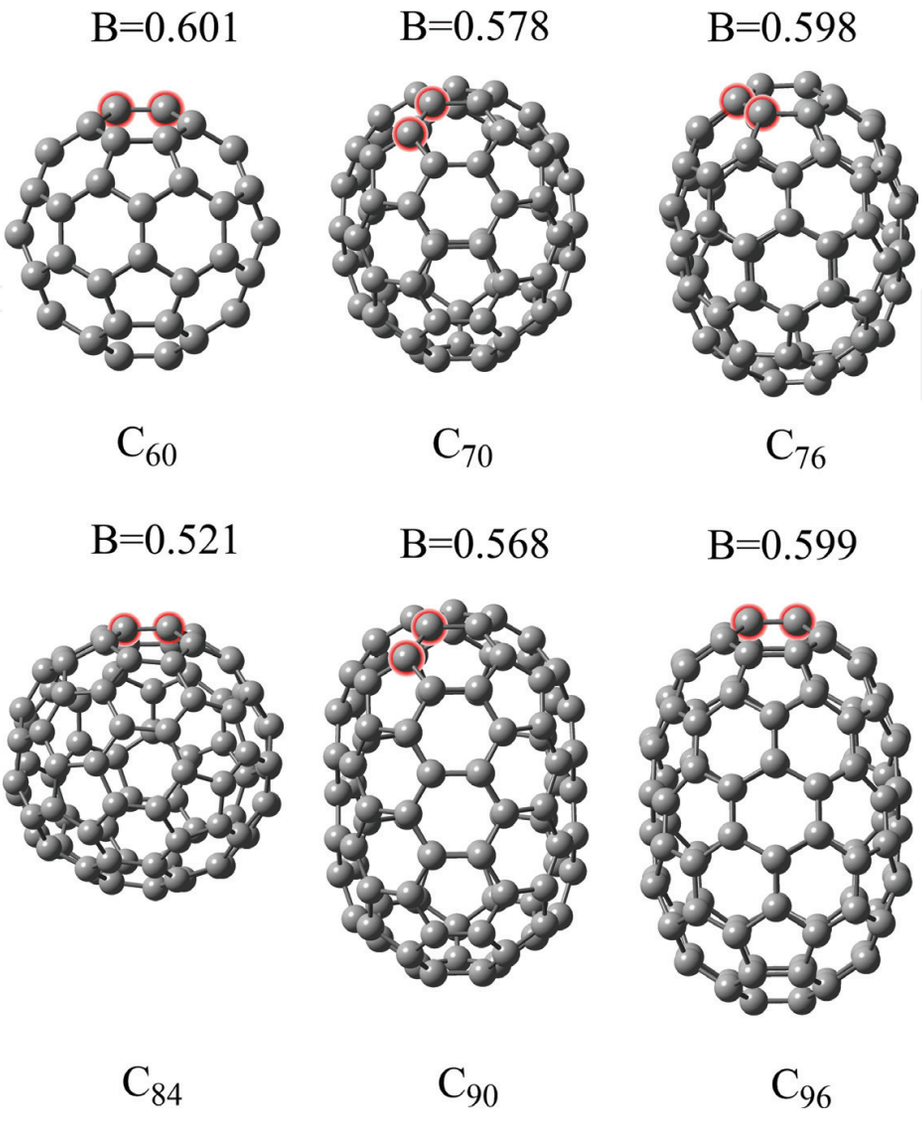

Scheme 1. The sites of attack for addition to the fullerenes Ih-C_{60}, D_{5h}-C_{70}, D_2-C_{76}, $D_{2d}(23)$-C_{84}, $D_{5h}(1)$-C_{90} and $D_{5h}(1)$-C_{96}. The Hückel π bond orders (B) were calculated using the freeware program, HuLiS [16].

The geometry optimizations are performed without any symmetry restrictions by using the M06 [17]/LANL2DZ [18, 19] level of theory. The vibrational frequency calculations at 298.15 K and 1 atm use the same level of theory. The stationary points are confirmed by the absence of imaginary frequencies. The natural charges are obtained using NBO 5.9, as implemented in the Gaussian 09 program [20].

The interatomic interactions are determined using energy decomposition analysis (EDA). Two types of EDA are used in this work. The first is the basic EDA that was developed individually by Yang et al. [21] and by Ziegler and Rauk [22]. For this basic EDA, the bonding energy (ΔE) is partitioned into two terms, ΔE = ΔE(DEF) + ΔE(INT). In this work, basic EDA is used for the optimized $ML_2X@C_n$ complexes, which are categorized into transition metal complexes (A), carbon cages (B) and metal ions (C) as shown in **Scheme 2**. The deformation energy (ΔE(DEF))

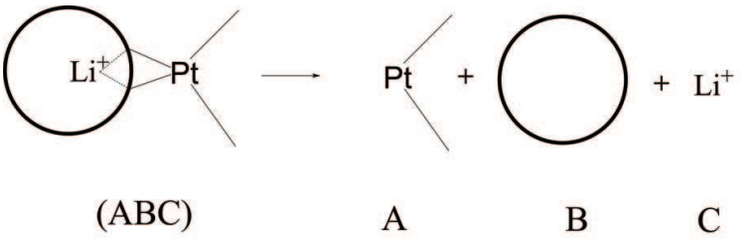

$$Ao+Bo+C \longrightarrow A+B+C \longrightarrow A+(BC) \longrightarrow (ABC)$$
$$\Delta E(DEF) \qquad \Delta E(INT)_{A(BC)}$$

$$\Delta E(DEF) = (E_A+E_B+E_C)-(E_{Ao}+E_{Bo}+E_C)$$
$$= (E_A-E_{Ao})+(E_B-E_{Bo})$$
$$= \Delta E(DEF)_A+\Delta E(DEF)_B$$
$$\Delta E(INT)_{A(BC)} = (E_{(ABC)})-(E_A+E_{(BC)})$$

Scheme 2. Basic EDA for $\{\eta^2\text{-}(Li^+@C_n)\}PtL_2$.

is the sum of the deformation energy of A ($\Delta E(DEF)_A$, which is defined as the energy of A in the product relative to the optimized isolated structure (A_0) and B ($\Delta E(DEF)_B$)). The interaction energy term, $\Delta E(INT)_{A(BC)}$, is the interaction energy between A and (BC) for their respective optimized product structures.

Advanced EDA unites the natural orbitals for chemical valence (NOCV), so it is possible to separate the total orbital interactions into pairwise contributions [23]. The advanced EDA (i.e., EDA-NOCV) further divides the interaction energy ($\Delta E(INT)$) into three main components: $\Delta E(INT) = \Delta E_{elstat} + \Delta E_{Pauli} + \Delta E_{orb}$. It is used for a quantitative study of π back-bonding to fullerene ligands that uses the M06/TZ2P level of theory with the ADF 2016 program package [24]. The relativistic effect is considered by applying a scalar zero-order regular approximation (ZORA) [25]. The interaction energy and its decomposition terms are obtained from a single-point calculation using the M06/TZ2P basis set from the Gaussian 09 optimized geometry.

3. Results and discussion

3.1. Geometric changes

The structures of $\{\eta^2\text{-}(X@C_n)\}ML_2$ complexes for M = Pt, Pd; X = F^-, 0, Li^+ and n = 60, 70, 76, 84, 90 and 96 were fully optimized at the M06/LANL2DZ level of theory. The geometries that are obtained are illustrated in **Figure 1**. The key structural parameters of the stationary points are listed in **Table 1** (the structural parameters for n = 70, 76, 84, 90 and 96 are presented elsewhere). For the Pt-C_{60} complex in the absence of encapsulated ions, the respective lengths of the metal-carbon bonds are 2.12 Å and 2.12 Å (**Table 1**). When the Li^+ ion is encapsulated into the cage, the metal-carbon bonds remain unaltered and the respective distances between

http://dx.doi.org/10.5772/intechopen.70068

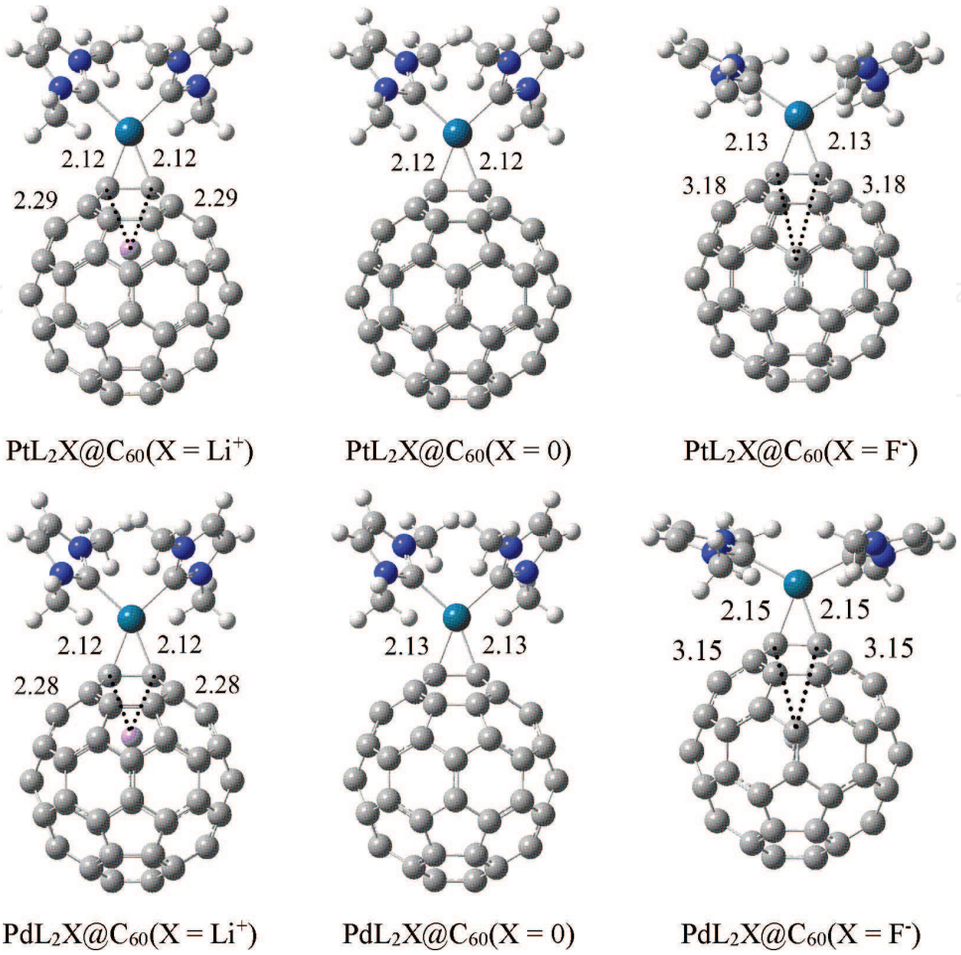

Figure 1. Optimized geometries for $\{\eta^2\text{-}(X@C_{60})\}ML_2$ (M = Pt, Pd; X = Li^+, 0, F^-).

C_1, C_2 and Li^+ are 2.29 Å and 2.29 Å. As the encapsulated ion is changed to F^-, the metal-carbon bonds remain almost unchanged (2.13 and 2.13 Å), but the distance between C_1, C_2 and encapsulated ions (F^-) increases (3.18 and 3.18 Å). The Li^+ ion is located at a site that is close to the transition metals because of electrostatic interaction. The metal-coordinated carbon atoms of C_{60} are negatively charged because there is π back-donation from the metal center. For the Pt-C_{60} complex without encapsulated ions, the natural population analysis (NPA) shows that the atomic charges on the C_1 (C_2) atoms are −0.27 (−0.27). When the cage is encapsulated by a Li^+ ion, the atomic charges on the C_1 (C_2) atoms are increased to −0.32 (−0.32) and the atomic charge on the Li atom is +0.86. Therefore, the encaged Li^+ ion is attracted toward these negatively charged C atoms. However, as the encapsulated ion is changed to F^-, NPA shows that the atomic charges on C_1 (C_2) atoms are decreased to −0.23 (−0.23) and the atomic charge on the F atom is negative (−0.93), so the encaged F^- ion is repelled by the negatively charged C atoms. In terms of Pd-C_{60} complexes, it is worthy of note that the geometrical distances are generally similar to the corresponding distances for Pt-C_{60} complexes, but the charge distributions are different. Specifically, the encaged Li atom has a charge (+0.86) but the charges on C_1 (C_2) atoms are reduced to −0.27 (−0.27). The negative charges on metal-coordinated carbon atoms are also less for X = 0 and F^-. Similar geometric changes and charge distributions are seen for n = 70, 76, 84, 90 and 96 and are presented elsewhere.

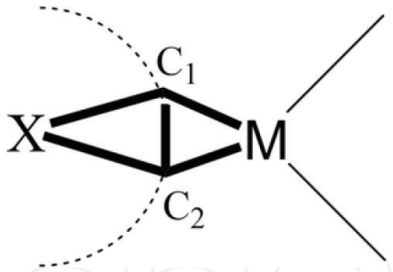

System	Geometrical parameters				NPA atomic charge			
	$M\text{-}C_1$	$M\text{-}C_2$	$X\text{-}C_1$	$X\text{-}C_2$	M	C_1	C_2	X
M = Pt; X = Li^+								
$ML_2X@C_{60}$	2.12	2.12	2.29	2.29	+0.48	−0.32	−0.32	+0.86
M = Pt; X = 0								
$ML_2X@C_{60}$	2.12	2.12	–	–	+0.46	−0.27	−0.27	–
M = Pt; X = F^-								
$ML_2X@C_{60}$	2.13	2.13	3.18	3.18	+0.43	−0.23	−0.23	−0.93
M = Pd; X = Li^+								
$ML_2X@C_{60}$	2.12	2.12	2.28	2.28	+0.44	−0.27	−0.27	+0.86
M = Pd; X = 0								
$ML_2X@C_{60}$	2.13	2.13	–	–	+0.40	−0.21	−0.21	–
M = Pd; X = F^-								
$ML_2X@C_{60}$	2.15	2.15	3.15	3.15	+0.34	−0.16	−0.16	−0.93

Table 1. Selected geometrical parameters (bond distances in Å) and the NPA atomic charge for optimized complexes ($\{\eta^2\text{-}(X@C_{60})\}ML_2$) at the M06/LANL2DZ level of theory.

3.2. Basic energy decomposition analysis (basic EDA)

In order to better understand the factors that govern the thermodynamic stability of $\{\eta^2\text{-}(X@C_n)\}ML_2$ complexes, basic EDA is performed on $\{\eta^2\text{-}(X@C_n)\}ML_2$ complexes (the basic EDA results for n = 70, 76, 84, 90 and 96 are presented elsewhere). The bonding energy (ΔE) is defined as $\Delta E = E(\{\eta^2\text{-}(X@C_n)\}ML_2) - E(X@C_n) - E(ML_2)$, using Eq. (1). The Pt-$C_{60}$ complex without encapsulated ions is initially considered. Basic EDA shows that both the metal fragment and the empty C_{60} fragment are distorted during the formation of the metal-carbon bond (**Table 2**). The metal fragment undergoes greater distortion ($\Delta E(DEF)_A$ = 52.1 kcal/mol) than C_{60} ($\Delta E(DEF)_B$ = 13.9 kcal/mol). The same results are obtained for X = Li^+ or F^-. It is found that the encapsulation of the Li^+ ion induces more distortion in fragments A and B of the Pt-$Li^+@C_{60}$ complex than those of the Pt-$F^-@C_{60}$ complex ($\Delta\Delta E(DEF)(X = Li^+)$ = 8.0, $\Delta\Delta E(DEF)(X = F^-)$ = −14.8 kcal/mol). However, the interaction energy increases when the Li^+ ion is encapsulated ($\Delta\Delta E(INT)_{A(BC)}(X = Li^+)$ = −35.9, $\Delta\Delta E(INT)_{A(BC)}(X = F^-)$ = +33.8 kcal/mol), which shows that the encapsulated Li^+ ion induces a stronger interaction between the metal fragment and the $X@C_{60}$ fragment, so $\{\eta^2\text{-}(Li^+@C_{60})\}PtL_2$

http://dx.doi.org/10.5772/intechopen.70068

X	ΔE(DEF) (ΔE(DEF)$_A$, ΔE(DEF)$_B$)	ΔΔE(DEF)[c]	ΔE(INT)$_{A(BC)}$	ΔΔE(INT)$_{A(BC)}$[c]	ΔE[d]	ΔΔE[c,d]
{η^2-(X@C_{60})}PtL_2						
F^-	51.2 (41.0, 10.2)	−14.8	−67.0	+33.8	−14.7	+20.1
0	66.0 (52.1, 13.9)	–	−100.8	–	−34.8	–
Li^+	74.0 (55.0, 19.0)	8.0	−136.6	−35.9	−64.2	−29.4
{η^2-(X@C_{60})}PdL_2						
F^-	30.7 (25.9, 4.8)	−12.6	−45.8	29.0	−13.9	+17.6
0	43.3 (35.0, 8.3)	–	−74.8	–	−31.5	–
Li^+	51.1 (37.9, 13.2)	7.8	−109.3	−34.5	−59.2	−27.7

[a]Energies are given in kcal/mol.

[b]A and B respectively represent the metal fragment and C_{60} cage.

[c]The difference is relative to corresponding quantity at X = 0.

[d]The reaction energy without zero-point energy (ZPE) correction for the product, relative to the corresponding reactants.

Table 2. Basic EDA for {η^2-(X@C_{60})}ML_2 (M = Pt, Pd) at M06/LANL2DZ[a,b].

is more stable. The relative thermodynamic stability increases in the order: ΔE(X = F^-) < ΔE (X = 0) < ΔE(X = Li^+), as shown in **Table 2**. In addition, |ΔΔE(DEF)| is small and |ΔΔE(INT)$_{A(BC)}$| is large, so the latter must be responsible for an increase in thermodynamic stability. Similar results are obtained for Pd-C_{60} complexes, but, the distortion in fragments A or B is smaller than that for the Pt-C_{60} complex, as is the interaction energy, so the complex is less stable. For instance, ΔE(M = Pd, X = Li^+) = −34.5 > ΔE(M = Pt, X = Li^+) = −35.9 kcal/mol. When the cage size increases (n = 70, 76, 84, 90 and 96), the encapsulated Li^+ ion still induces a stronger interaction between the metal fragment and the X@C_n fragment and |ΔΔE(DEF)| is smaller than |ΔΔE(INT)$_{A(BC)}$|. Therefore, an increase in the cage size has no effect on the basic EDA results.

3.3. Advanced energy decomposition analysis (advanced EDA)

In an earlier study by the authors, structural parameters and spectral characteristics were used to estimate the strength of π back-bonding for {η^2-(X@C_{60})}ML_2 (M = Pt, Pd; X = 0, Li^+, L = PPh_3) complexes [10]. The changes in bond length ($\Delta r/r_0$), bond angle ($\Delta\theta_{av}$), vibrational frequency (Δν) and the chemical shift (Δδ) were used to describe the character of the π-complex s. In this study, the strength of the π back-bonding strength is estimated from an energetic viewpoint using an advanced EDA method. This analysis shows the effect of encapsulated ions, metal fragments and cage sizes on π back-bonding.

3.3.1. The effect of encapsulated ions on π back-bonding

In an earlier discussion (Section 3.2), it was proven that thermodynamic stabilities increase in the order: ΔE(X = F^-) < ΔE(X = 0) < ΔE(X = Li^+), because the interaction energy (ΔE(INT))

is increased. The interaction between the metal fragment and $X@C_n$ is now studied using advanced EDA, which further decomposes the interaction energy into electrostatic interaction (ΔE_{elstat}), repulsive Pauli interaction (ΔE_{Pauli}) and orbital interaction (ΔE_{orb}) terms. The orbital interactions are the most important of these three and only the most important pairwise contributions to ΔE_{orb} are considered. The advanced EDA method is used for $\{\eta^2\text{-}(X@C_n)\}ML_2$ complexes, as shown in **Tables 3** and **4** (the results for n = 70, 76, 84, 90 and 96 are presented elsewhere). A plot of the deformation density and a qualitative drawing of the orbital interactions between the metal fragment and $X@C_{60}$ are shown in **Figure 2**. In terms of the Pt-C_{60} complexes, **Table 3** shows that both the electrostatic interaction (ΔE_{elstat}) and the orbital interaction (ΔE_{orb}) stabilize the complexes because they are negative terms, but the percentage of ΔE_{orb} increases in the order: $\Delta E_{orb}(X = F^-) < \Delta E_{orb}(X = 0) < \Delta E_{orb}(X = Li^+)$. Therefore, the enhanced orbital interaction must be responsible for the increase in the thermodynamic stability. **Table 3** also shows that ΔE_1 contributes significantly to ΔE_{orb}: 69.5% for $X = F^-$, 75.2% for X = 0 and 76.4% for $X = Li^+$. The deformation densities show that these come from π back-donation from a filled *d* orbital of the metal to the π* orbitals of C_{60} (charge flow is yellow to green at the top of **Figure 2c**). The large contributions of ΔE_1 to ΔE_{orb} are in agreement with the results of previous studies. The metal-carbon bonds are principally formed by π back-donation [8]. It is also seen that the order of ΔE_1 is $|\Delta E_1(X = F^-)| = 94.4 < |\Delta E_1(X = 0)| = 118.6 < |\Delta E_1(X = Li^+)| = 142.8$ kcal/mol. Therefore, ΔE_1 is increased when there is the encapsulated Li^+ ion but decreased when there is a F^- ion. The second contribution of ΔE_2 to ΔE_{orb} is comparatively small: 18.0% for $X = F^-$, 13.1% for X = 0 and 10.0% for $X = Li^+$. This results from

Fragments	L_2Pt and $F^-@C_{60}$	L_2Pt and C_{60}	L_2Pt and $Li^+@C_{60}$
ΔE_{int}	−67.7	−100.8	−133.0
ΔE_{Pauli}	257.2	235.8	227.6
ΔE_{elstat}[b]	−189.0 (58.2%)	−178.8 (53.1%)	−173.8 (48.2%)
ΔE_{orb}[b]	−135.8 (41.8%)	−157.7 (46.9%)	−186.9 (51.8%)
ΔE_1[c]	−94.4 (69.5%)	−118.6 (75.2%)	−142.8 (76.4%)
ΔE_2[c]	−24.4 (18.0%)	−20.6 (13.1%)	−18.6 (10.0%)
ΔE_3[c]	−7.1 (5.2%)	−5.7 (3.6%)	−6.5 (3.5%)
ΔE_4[c]	−3.0 (2.2%)	−3.8 (2.4%)	−5.5 (3.0%)
ΔE_5[c]	−3.6 (2.7%)	−4.2 (2.7%)	−5.0 (2.7%)
ΔE_6[c]	–	–	−2.1 (1.1%)
ΔE_{rest}[c]	−5.8 (4.3%)	−6.3 (4.0%)	−6.8 (3.6%)

[a]Optimized structures at the M06/LANL2DZ level of theory.

[b]The values in parentheses give the percentage contribution to the total attractive interactions, $\Delta E_{elstat} + \Delta E_{orb}$.

[c]The values in parentheses give the percentage contribution to the total orbital interactions, ΔE_{orb}.

Table 3. The advanced EDA results for $\{\eta^2\text{-}(X@C_{60})\}PtL_2$[a] (X = F^-, 0, Li^+) at the M06/TZ2P level of theory. The fragments are PtL_2 and $X@C_{60}$ in a singlet (S) electronic state. All energy values are in kcal/mol.

Fragments	L_2Pd and $F^-@C_{60}$	L_2Pd and C_{60}	L_2Pd and $Li^+@C_{60}$
ΔE_{int}	−45.1	−73.5	−103.9
ΔE_{Pauli}	188.9	176.5	176.4
ΔE_{elstat} [b]	−142.8 (61.0%)	−137.0 (54.8%)	−138.9 (49.6%)
ΔE_{orb} [b]	−91.2 (39.0%)	−113.0 (45.2%)	−141.3 (50.4%)
ΔE_1 [c]	−71.9 (78.8%)	−96.9 (85.8%)	−121.0 (85.6%)
ΔE_2 [c]	−15.5 (17.0%)	−10.8 (9.6%)	−9.4 (6.7%)
ΔE_3 [c]	−4.9 (5.4%)	−4.2 (3.7%)	−4.6 (3.3%)
ΔE_4 [c]	−2.1 (2.3%)	−2.3 (2.0%)	−3.6 (2.5%)
ΔE_5 [c]	−2.0 (2.2%)	−2.9 (2.6%)	−3.6 (2.5%)
ΔE_{rest} [c]	−2.7 (3.0%)	−3.6 (3.2%)	−6.5 (4.6%)

[a]Optimized structures at the M06/LANL2DZ level of theory.

[b]The values in parentheses give the percentage contribution to the total attractive interactions, $\Delta E_{elstat} + \Delta E_{orb}$.

[c]The values in parentheses give the percentage contribution to the total orbital interactions, ΔE_{orb}.

Table 4. The advanced EDA results for $\{\eta^2\text{-}(X@C_{60})\}PdL_2$ [a] ($X = F^-$, 0, Li^+) at the M06/TZ2P level of theory. The fragments are PdL_2 and $X@C_{60}$ in the singlet (S) electronic state. All energy values are in kcal/mol.

σ-donation from a filled π orbital of C_{60} to the π* orbital of the metal (middle of **Figure 2c**). The computational results show that π back-bonding is crucial to the thermodynamic stability of Pt-C_{60} complexes and that an encapsulated Li^+ ion increases π back-bonding but an encapsulated F^- has the opposite effect.

3.3.2. The effect of metal fragments on π back-bonding

Pd-C_{60} complexes appear to be similar to Pt-C_{60} complexes, but a comparison of the results in **Tables 3** and **4** shows that the value ΔE_1 for a Pd-C_{60} complex is smaller than the corresponding value for a Pt-C_{60} complex, which demonstrates that the π back-bonding for a palladium center is weaker than that for a platinum center. For example, $|\Delta E_1(M = Pd, X = Li^+)| = 121.0 < |\Delta E_1(M = Pt, X = Li^+)| = 142.8$ kcal/mol. This is consistent with the earlier results that were obtained using structural parameters and spectral characteristics [10].

3.3.3. The effect of cage sizes on π back-bonding

Figure 3 shows a plot of the ΔE_1 values versus cage sizes that are calculated for $\{\eta^2\text{-}(X@C_n)\}PtL_2$ complexes (n = 60, 70, 76, 84, 90 and 96). It is seen that there is no linear relationship and there is one obvious peak for each X at n = 84 [26]. This demonstrates the effect of a difference in size of the carbon clusters on π back-bonding for a metal center, but the correlation is not simply monotonic. Therefore, a larger (smaller) cage size does not necessarily imply that there is stronger (weaker) π back-bonding, which results in greater (lower) thermodynamic stability.

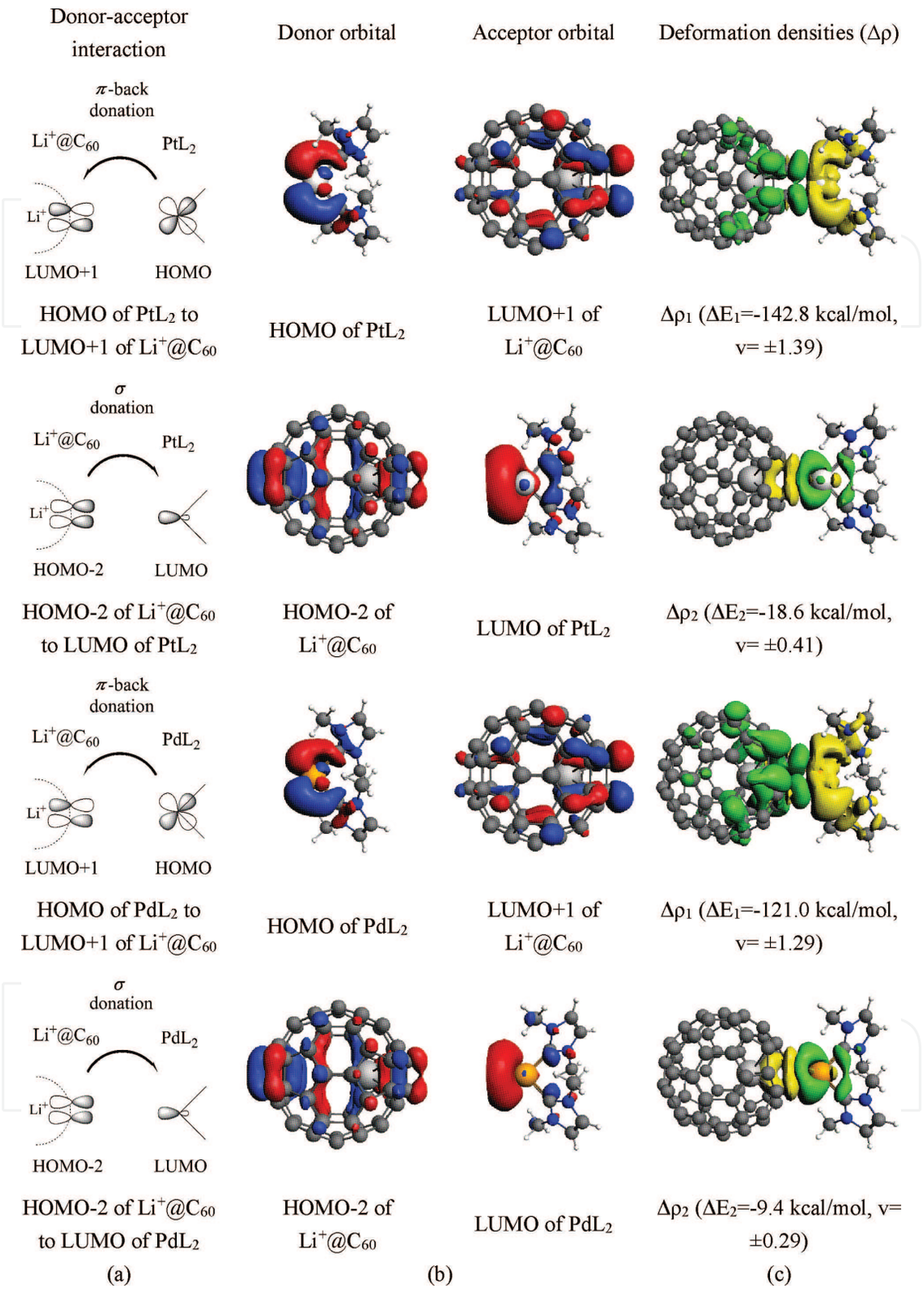

Figure 2. (a) A qualitative drawing of the orbital interactions between the metal fragment and $Li^+@C_{60}$; (b) the shape of the most important interacting occupied and vacant orbitals of the metal fragments and $Li^+@C_{60}$; (c) a plot of the deformation densities, Δρ, for the pairwise orbital interactions between the two fragment in their closed-shell state, the associated interaction energies, ΔE_{orb} (in kcal/mol), and the eigenvalues ν. The eigenvalues, ν, indicate the size of the charge flow. The direction of the charge flow is from yellow to the green.

http://dx.doi.org/10.5772/intechopen.70068

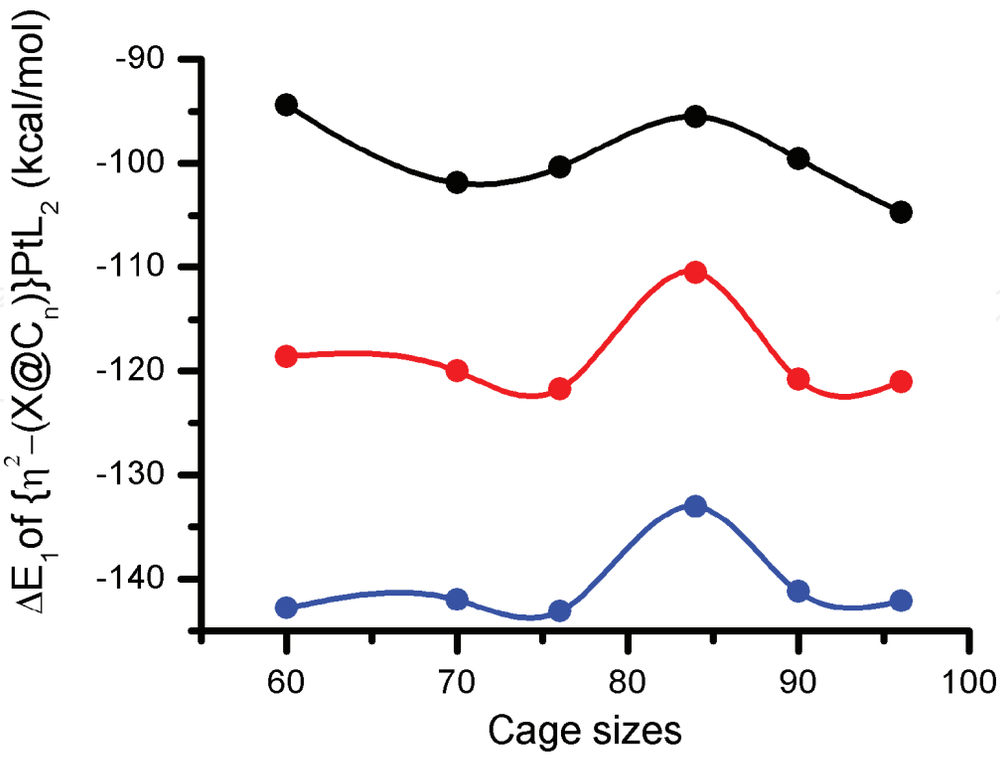

Figure 3. The correlation between ΔE_1 and cage sizes for $\{\eta^2\text{-}(X@C_n)\}PtL_2$ (n = 60, 70, 76, 84, 90 and 96) complexes. The blue, red and black lines indicate the ΔE_1 for X = Li^+, 0 and F^-, respectively.

4. Conclusion

This computational study uses density functional theory to determine the thermodynamic stability of $\{\eta^2\text{-}(X@C_n)\}ML_2$ complexes (M = Pt, Pd; X = F^-, 0, Li^+ and n = 60, 70, 76, 84, 90 and 96). The calculations show the reaction is more stable when the Li^+ ion is encapsulated within C_n but the complex becomes unstable if there is a F^- ion. Basic EDA shows that there is an increase in the interaction between the metal fragment and C_n if there is an encapsulated Li^+ ion but F^- ion has the opposite effect.

The advanced EDA results show that π back-bonding is crucial to thermodynamic stability and that thermodynamic stability is increased by the presence of a Li^+ ion but the presence of a F^- ion has the opposite effect. These computations also show that a platinum center results in stronger π back-bonding than a palladium center and that there is no linear relationship between cage size and π back-bonding.

Acknowledgements

The authors would like to thank the National Center for High-Performance Computing in Taiwan for the donation of generous amounts of computing time. The authors are also grateful for financial support from the Ministry of Science and Technology of Taiwan.

Author details

Ming-Chung Yang[1] and Ming-Der Su[1,2]*

*Address all correspondence to: midesu@mail.ncyu.edu.tw

1 Department of Applied Chemistry, National Chiayi University, Chiayi, Taiwan

2 Department of Medicinal and Applied Chemistry, Kaohsiung Medical University, Kaohsiung, Taiwan

References

[1] Fagan PJ, Calabrese JC, Malone B. The chemical nature of buckminsterfullerene (C_{60}) and the characterization of a platinum derivative. Science. 1991;**252**:1160-1161. DOI: 10.1126/science.252.5009.1160

[2] Lebedeva MA, Chamberlain TW, Khlobystov AN. Harnessing the synergistic and complementary properties of fullerene and transition-metal compounds for nanomaterial applications. Chemical Reviews. 2015;**115**:11301-11351. DOI: 10.1021/acs.chemrev.5b00005

[3] Balch AL, Catalano VJ, Lee JW. Accumulating evidence for the selective reactivity of the 6-6 ring fusion of C_{60}. Preparation and structure of $(\eta^2\text{-}C_{60})Ir(CO)Cl(PPh_3)_2{\cdot}5C_6H_6$. Inorganic Chemistry. 1991;**30**:3980-3981. DOI: 10.1021/ic00021a003

[4] Balch AL, Costa DA, Noll BC, Olmstead MM. Oxidation of buckminsterfullerene with m-chloroperoxybenzoic acid. Characterization of a Cs isomer of the diepoxide $C_{60}O_2$. Journal of the American Chemical Society. 1995;**117**:8926-8932. DOI: 10.1021/ja00140a005

[5] Balch AL, Winkler K. Two-component polymeric materials of fullerenes and the transition metal complexes: A bridge between metal−organic frameworks and conducting polymers. Chemical Reviews. 2016;**116**:3812-3882. DOI: 10.1021/acs.chemrev.5b00553

[6] Tsikalova MV, Zheludkov SV, Vorontsov EI, Bashilov VV, Babievskii KK, Sokolov VI, Novikov YN. Optically active rhodium and iridium C_{60} complexes containing the enantiomeric ligand (+)DIOP: $(\eta^2\text{-}C_{60})MH(CO)[(+)DIOP]$ (M = Rh, Ir). Mendeleev Communications. 2011;**21**:256. DOI: 10.1016/j.mencom.2011.09.008

[7] Proft FD, Alsenoy CV, Geerlings P. Ab initio study of the endohedral complexes of C_{60}, Si_{60}, and Ge_{60} with monoatomic ions: Influence of electrostatic effects and hardness. The Journal of Physical Chemistry. 1996;**100**:7440-7448. DOI: 10.1021/jp960174w

[8] Watanabe T, Itoh MF, Komuro T, Okada H, Sakai T, Ono Y, Kawachi K, Kasama Y, Tobita H. Iridium and platinum complexes of $Li^+@C_{60}$. Organometallics. 2014;**33**:608-611. DOI: 10.1021/om4008899

[9] Simoes JAM, Beauchamp JL. Transition metal-hydrogen and metal-carbon bond strengths: The keys to catalysis. Chemical Reviews. 1990;**90**:629-688. DOI: 10.1021/cr00102a004

[10] Yang MC, Sharma AK, Sameera WMC, Morokuma K, Su MD. A theoretical study of addition reactions of L_4M(M = Rh, Ir) and L_2M(M = Pd, Pt) to $Li^+@C_{60}$. The Journal of Physical Chemistry A. 2017;**121**:2665-2673. DOI: 10.1021/acs.jpca.7b01086

[11] Hopkinson MN, Richter C, Schedler M, Glorius F. An overview of N-heterocyclic carbenes. Nature. 2014;**510**:485-496. DOI: 10.1038/nature13384

[12] Balch AL, Olmstead MM. Reactions of transition metal complexes with fullerenes (C_{60}, C_{70}, etc.) and related materials. Chemical Reviews. 1998;**98**:2123-2165. DOI: 10.1021/cr960040e

[13] Yang H, Beavers CM, Wang Z, Jiang A, Liu Z, Jin H, Mercado BQ, Olmstead MM, Balch AL. Isolation of a small carbon nanotube: The surprising appearance of $D_{5h}(1)$-C_{90}. Angewandte Chemie International Edition. 2009;**48**:1-6. DOI: 10.1002/anie.200906023

[14] Yang H, Jin H, Che Y, Hong B, Liu Z, Gharamaleki JA, Olmstead MM, Balch AL. Isolation of four isomers of C_{96} and crystallographic characterization of nanotubular $D_{3d}(3)$-C_{96} and the somewhat flat-sided sphere $C_2(181)$-C_{96}. Chemistry—A European Journal. 2012;**18**:2792-2796. DOI: 10.1002/chem.201103852

[15] Fowler PW, Manolopoulos DE. An Atlas of Fullerenes. Oxford: Clarendon; 1995. DOI: http://dx.doi.org/10.1080/10641229608001575

[16] Hagebaum-Reignier D, Girardi R, Carissan Y, Humbel S. Hückel theory for Lewis structures: Hückel–Lewis Configuration Interaction (HL-CI). Journal of Molecular Structure: THEOCHEM. 2007;**817**:99-109. DOI: 10.1016/j.theochem.2007.04.026

[17] Zhao Y, Truhlar DG. The M06 suite of density functionals for main group thermochemistry, thermochemical kinetics, noncovalent interactions, excited states, and transition elements: Two new functionals and systematic testing of four M06-class functionals and 12 other functionals. Theoretical Chemistry Accounts. 2008;**120**:215-241. DOI: 10.1007/s00214-007-0310-x

[18] Dunning TH, Hay PJ. In: Schaefer HF, editor. Modern Theoretical Chemistry. Vol. 3. New York: Plenum; 1977. pp. 1-28

[19] Hay PJ, Wadt WR. Ab initio effective core potentials for molecular calculations—Potentials for the transition-metal atoms Sc to Hg. The Journal of Chemical Physics. 1985;**82**:270-283. DOI: http://dx.doi.org/10.1063/1.448799

[20] Frisch MJ, Trucks GW, Schlegel HB, Scuseria GE, Robb MA, Cheeseman JR, Scalmani G, Barone V, Mennucci B, Petersson GA, et al. Wallingford, CT: Gaussian, Inc.; 2013

[21] Sameera WMC, Hatanaka M, Kitanosono T, Kobayashi S, Morokuma K. The mechanism of iron(II)-catalyzed asymmetric Mukaiyama aldol reaction in aqueous media: Density functional theory and artificial force-induced reaction study. Journal of the American Chemical Society. 2015;**137**:11085-11094. DOI: 10.1021/jacs.5b05835

[22] Ziegler T, Rauk A. Carbon monoxide, carbon monosulfide, molecular nitrogen, phosphorus trifluoride, and methyl isocyanide as σ donors and π acceptors. A theoretical study by the Hartree-Fock-Slater transition-state method. Inorganic Chemistry. 1979;**18**:1755-1759. DOI: 10.1021/ic50197a006

[23] Zhao L, Jones C, Frenking G. Reaction mechanism of the symmetry-forbidden [2+2] addition of ethylene and acetylene to amido-substituted digermynes and distannyes Ph_2N-EE-NPh_2, (E = Ge, Sn). A theoretical study. Chemistry–A European Journal. 2015;**21**:12405-12413. DOI: 10.1002/chem.201501457

[24] Bickelhaupt FM, Baerends EJ. Kohn-Sham density functional theory: Predicting and understanding chemistry. Reviews in Computational Chemistry. Wiley-VCH, New York. 2000;**15**:1-86

[25] Lenthe EV, Baerends EJ, Snijders JG. Relativistic regular two-component Hamiltonians. The Journal of Chemical Physics. 1993;**99**:4597-4610. DOI: http://dx.doi.org/10.1063/1.466059

[26] The reason for such a phenomenon is still unclear. Presumably, it would be because of the smallest Hückel π bond order (B = 0.521) for n = 84. The small π bond order is expected to be inactive, thus, leading to weak π back-bonding interaction. Further calculations are working on and will be present elsewhere